CHAPTER 2

Experimental techniques:

2.1 INTRODUCTION

Liquid crystals have fascinating physical and electro-optical properties and have been explored by different group of scientists throughout the globe since their importance was understood from the application point of view. In order to apply them in the display and other devices, it is very much essential to characterize their properties by measuring some parameters which are defined and expressed in terms of some other measurable parameters based on well established models. The measurements of these parameters are accomplished with some instruments with some special techniques. In this chapter we present the techniques used in the preparation of sample cells, instruments involved and the methodology in different experimental measurements such as – the identification of phases, methods used for the determination of material constants, dielectric measurements, determination of electro-optic parameters, etc.

The following experimental techniques are employed in this dissertation:

(i) Polarizing Optical Microscopy (POM)
(ii) Differential Scanning Calorimetry (DSC)
(iii) Molecular modeling.
(iv) Synchrotron X-ray diffraction Technique
(v) Frequency Domain Dielectric Spectroscopy (FDDS).
(vi) Electro-optic measurements which include – the measurement of tilt angle (θ), spontaneous polarization (Ps), switching Time (τ), rotational viscosity (γ), etc.

2.2 IDENTIFICATION OF MESOPHASES AND DETERMINATION OF TRANSITION TEMPERATURES

The primary and key task to characterize a liquid crystalline sample is to identify its mesophases and to determine the phase transition temperatures. Liquid crystalline materials may have different mesophases in between the crystalline solid and isotropic phase. There are several techniques to identify these mesophases and to determine the phase transition temperatures. These are – (i) Polarization optical microscopy (POM) [**1**], (ii) Differential scanning calorimetry (DSC) [**2**], (iii) X-ray diffraction [**3-4**], (iv) Frequency domain dielectric spectroscopy (FDDS) [**5**], (v) Neutron scattering techniques [**6**], (vi) Nuclear magnetic resonance (NMR) [**6-8**],

(vii) Raman Scattering [**9**], (viii) UV–visible spectroscopic studies [**10**], (ix) Fabry-Perot Etalon method [**11**], etc. Often these techniques give complementary information. We have employed only the first four techniques in this dissertation.

2.2.1 POLARIZING OPTICAL MICROSCOPY

Polarizing optical microscopy is a very useful tool to identify mesophases and to determine the transition temperatures. In this method, the liquid crystalline samples are sandwiched between a microscope glass slide and a glass cover slip and set in a hot stage, the temperature of which is controlled using a Mettler Toledo FP90 central processor with accuracy $\pm$ 0.1^{o}C within range of room temperature to 300^{o}C. The hot stage (Mettler FP82) is placed under the microscope and the polarizer is set at crossed position (90^{o}) with the analyzer. The temperature of the hot stage can be increased or decreased in a regulated manner and the textures are observed through the eyepiece of the microscope. There is also an arrangement to observe the textures on the monitor of a computer (PC) by fitting a Moticam 2500 digital camera on the top of the microscope and interfacing it with the PC using Moticam 2.0 software. The textures of the sample can be saved in photo or video mode using this software.

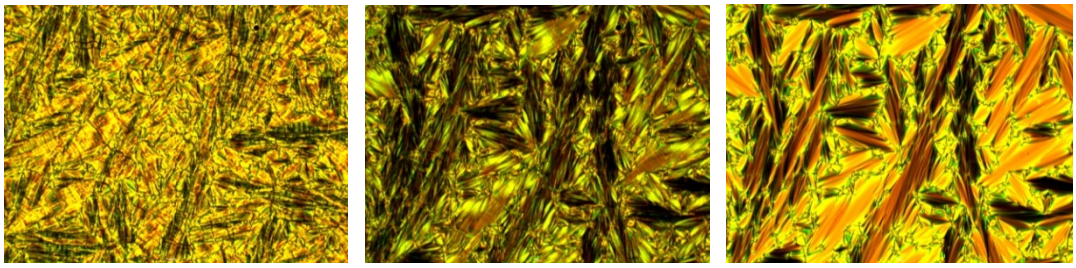

(a) SmC_A* (b) SmC* (c) SmA*

Figure 2.1. (a) Texture of (a) SmC_A* phase, (b) SmC* phase, and (c) SmA* phase

When a liquid crystalline sample is observed under a polarizing microscope, colourful gorgeous visual pattern is observed and this pattern is nothing but the defect structure of molecules in the long-range order. This visual pattern is called texture. A particular mesophase has its characteristics texture; however, a particular phase may exhibit more than one type of textures depending on the surface treatment of the glasses, thickness of the samples and thermal history. When the sample is heated or cooled the molecules of the sample change their conformation and hence change the defect structures. This change of defect structure in the long-range molecular order

takes place at specific temperatures and is manifested in the visual pattern of the polarizing microscope is called the change of phase and the corresponding temperature is recorded as phase transition temperature. Many books with standard photographs of typical textures of a huge variety of mesophases with their origins have been published by Demus and Richter (1978) [**12**], Bouligand *et al*. [**13**], Slaney *et al.*[**14**], I. Dierking [**1**]. The identification of mesophases is done by comparing the observed textures with those given in these standard books. The block diagram of the polarizing optical microscopy is shown in **Figure 2.2.**

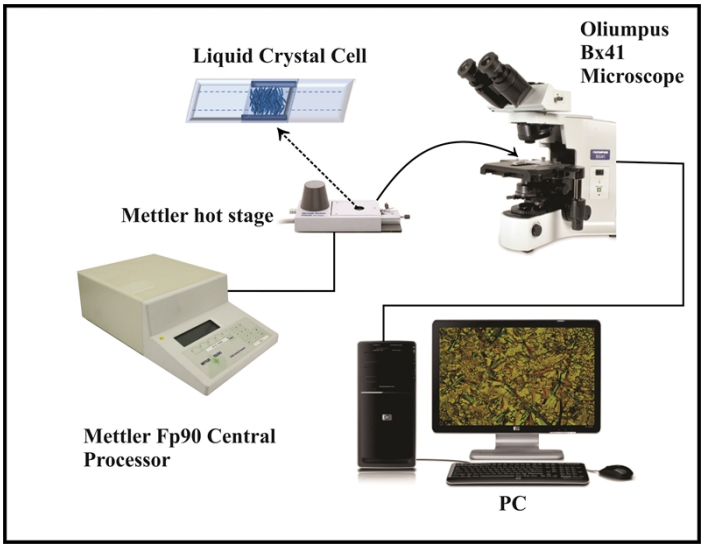

Figure 2.2. Block diagram of polarizing optical microscopy.

2.2.2 DIFFERENTIAL SCANNING CALORIMETRY

Differential Scanning Calorimetry (DSC), is a thermal analysis technique, that looks at how a material's enthalpy (ΔH) is changed at the transition temperature. This analysis measures the amount of energy absorbed or released by a sample when it is heated or cooled, providing quantitative and qualitative data on endothermic (heat absorption) and exothermic (heat evolution) processes. A sample of known mass is heated or cooled and the changes in its heat capacity are tracked as changes in the heat flow. In this technique the sample is placed in a suitable pan (of Al, Cu, Au, Pt, etc., we have used Al pan) and sits upon a constantan disc on a platform in the DSC analysis cell with chromel wafer immediately underneath. A chromel-alumel thermocouple under the constantan disc measures the sample temperature. An empty reference pan sits on a symmetric platform with its underlying chromel wafer and

chromel-alumel thermocouple. Heat flow is measured by comparing the difference in temperature across the sample and the reference chromel wafers. Mettler FP84 hot stage and Mettler FP90 central processor interfaced with a PC through FP99A software were used for DSC studies in our laboratory. The temperature run was given during heating and cooling at a specific scan rate (mostly 3^{o}C per minute) and the thermogram was recorded in a PC automatically. The block diagram of the experimental arrangement is shown in **Figure 2.3**. When a phase transition of a material takes place, change of enthalpy also takes place and this change of enthalpy is qualitatively and quantitatively represented in the thermogram by an anomaly. The level of enthalpy change provides some indication about the nature of the phase transition.

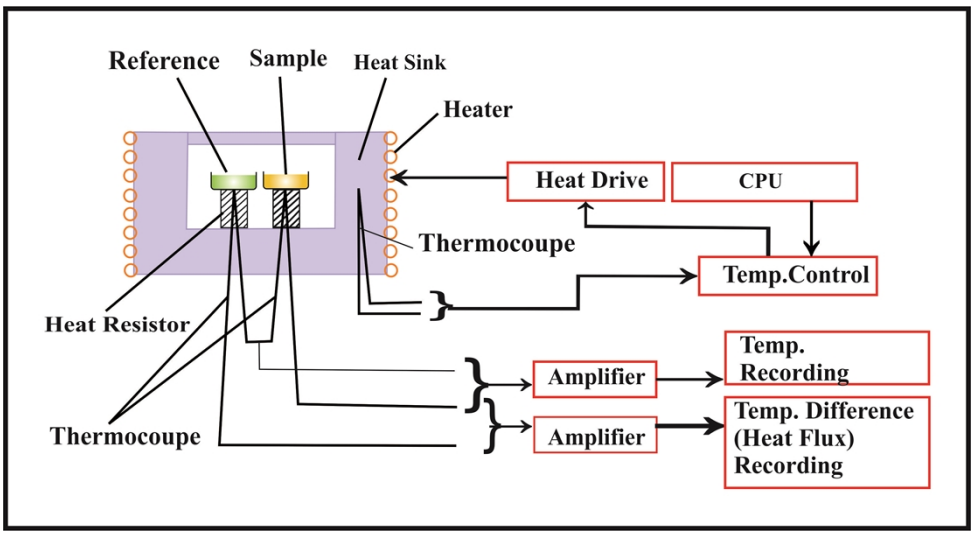

Figure 2.3. The Experimental set up of DSC experiment [**15**].

Crystal to liquid crystal transition involves high energy of transition. It means that the large changes in transition enthalpies are related to structural changes at phase transition [**16**]. Usually, crystal to N or SmA transitions, N or SmA to isotropic transitions are first order and they are prominent although liquid crystal to isotropic liquid transition is less prominent than crystal to liquid crystal phase transition. But crystal to higher-order smectics (like SmG) and phase changes within them are weakly first order or second order in nature and not always detectable by DSC techniques or sometimes maybe better observed by choosing proper heating and cooling rate [**17**]. The typical DSC plot is shown in **Figure 2.4**.

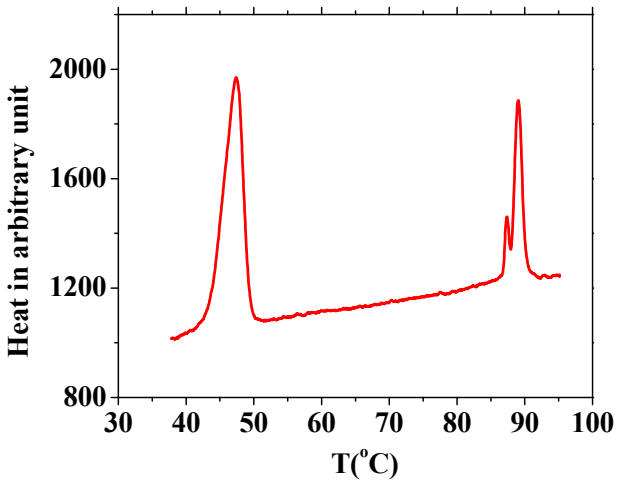

Figure 2.4. A typical DSC thermogram

2.3 DETERMINATION OF STRUCTURAL PARAMETERS USING THE X-RAY DIFFRACTION TECHNIQUE.

X-ray diffraction is the most reliable technique for investigation of the microscopic structure of liquid crystals. Details of this technique have been reviewed by many authors [**18-21**]. It maps the positions of the molecules in a particular phase and produces a typical diffraction pattern. From the knowledge of the structure of diffraction patterns over the temperature range, the phases present in the mesophase can be identified [**22-31**]. The alignment of the sample is done by applying a magnetic or an electric field in nematic LCs and by slow cooling in smectic LCs. The remarkable features of the x-ray diffraction pattern of nematic or smectic phases, which are obtained on normal incidence of the X-ray beam to the director **n** are one outer halo and one inner halo (**Figure 2.5**).

For unaligned samples the halos are uniform but in aligned samples the outer halo is split into two crescents showing maxima along equatorial direction perpendicular to **n** (or **H**, aligning magnetic field) (**Figure 2.5**), which are formed due to intermolecular scattering [**32**] and the corresponding angle gives a measure of average intermolecular distance between elongated molecules (D) (**Figure 2.5 (a)**). Similarly, the inner halo splits into two crescents with maxima at much lower angle in the meridional direction parallel to **n** (or **H**). These crescents are formed due to the molecular layer arrangement along **n [32]**. In smectic phases the inner pattern appears

as sharp spots, sometimes second order spots are also observed (**Figure 2.5 (b and c)**).

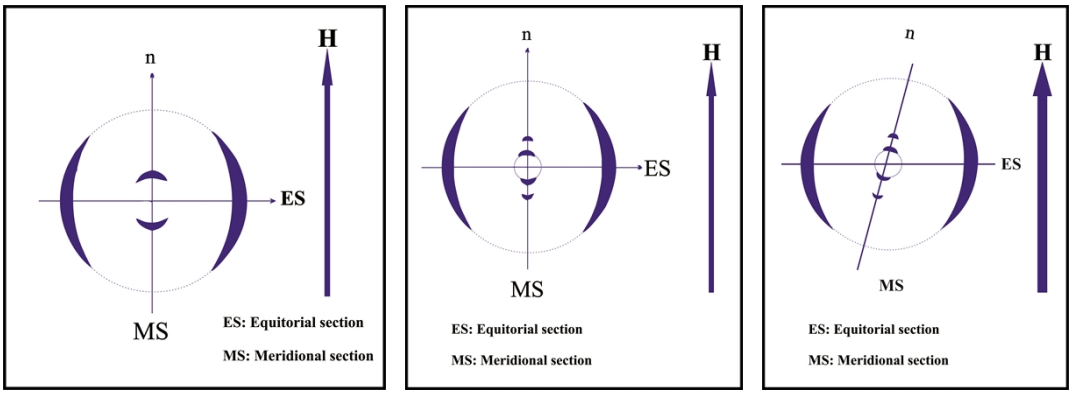

(a) (b) (c)

Figure 2.5. Schematic representation of typical X-ray diffraction pattern of an aligned (a) nematic phase and (b) Smectic–A phase and (c) Smectic–C phase (X-ray beam is perpendicular to the paper)

The low and high angle diffraction peaks were fitted to a Lorentzian and measuring the corresponding angle of diffraction from the fitted the apparent molecular length (l) (in nematics) or layer spacing (d) (in smectics) can be determined using Bragg equation

$$2d\,sin\theta = \lambda \tag{2.1}$$

where λ is the wavelength of the X-ray beam. But the average intermolecular distance (D) is determined using the modified Bragg formula [**32**],

$$2D\,sin\theta = 1.117\lambda \tag{2.2}$$

Estimated measurement error in d and D are 0.02 Å and 0.002 Å respectively.

Chiral smectic phases give rise to a similar diffraction pattern. It is worth to mention here in conventional X-ray scattering experiment it is not possible to distinguish smectic liquid crystal phases that differ with respect to the orientation (but not packing) of the molecules in successive layers like in SmC_A* and SmC* phases (possible by resonant X-ray scattering experiment, not done in this dissertation) **[33]**

In order to explore the structure of the pure antiferroelectric samples, the diffraction experiments were performed using a synchrotron radiation facility (PETRA III beamline at P07 Physics Hutch station) at Deutsches Elektronen Synchrotron, Hamburg, Germany. The samples were taken in the Lindeman glass tube

of 1.0 mm diameter by capillary action. The synchrotron radiation beam was passed normal geometry. The temperature of the sample was decreased very slowly to the desired temperature to get better alignment. A Perkin Elmer 2D detector of pixel size 200x200 μm^2 and total size 400x400 mm^2 was used for image grabbing which was placed at 3.3m away from the sample (**Figure 2.6**). 50 images of exposure time 0.2s were grabbed and averaged to get one diffraction image and two such images were collected at a particular temperature. All the physical parameters were averaged over these two image data. QXRD program for PE Area Detector (G. Jennings, version 9.8, 64 bit) was used for data acquisition and also for analyzing the image. Images were integrated using a step size of 0.002 to get the intensity versus scattering wave vector (Q) distribution. Experiments were also done by taking LC samples in dielectric cells and the electric field was applied but not presented in this dissertation.

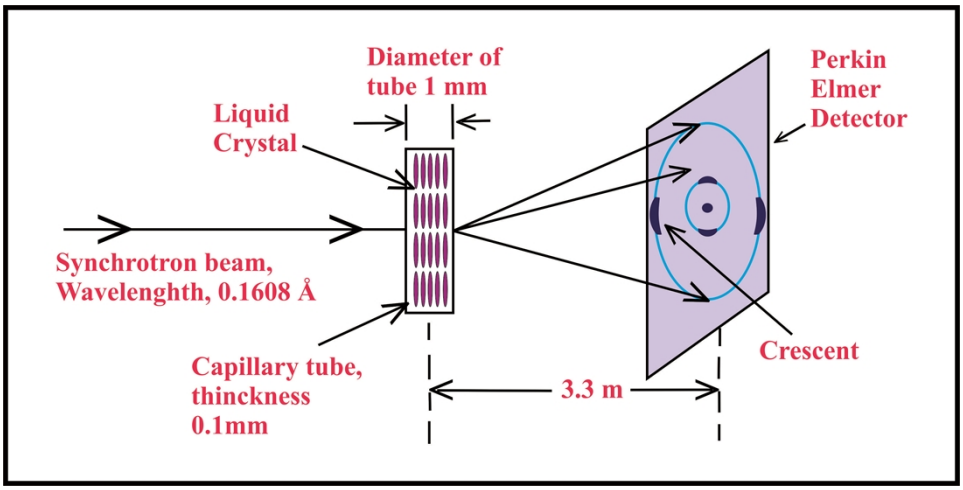

Figure 2.6. Schematic diagram of experimental arrangement of X-ray diffraction study (not to scale)

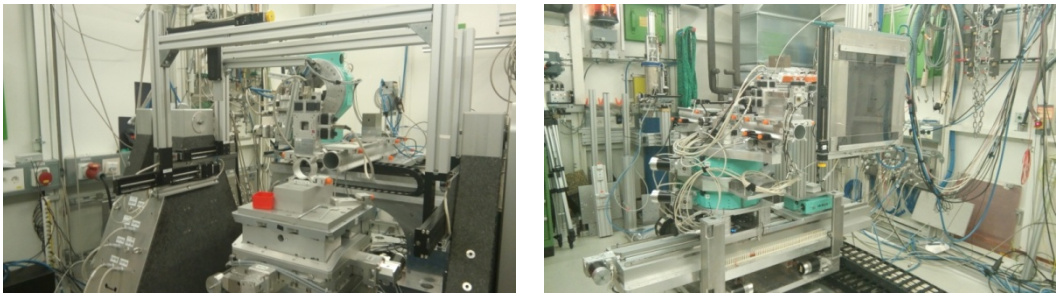

Figure 2.7.(a) Synchrotron X-ray diffraction set up unit (b) Perkin Elmer 2D detector of size 400x400 mm^2, at DESY, Hamburg, Germany

Under rigid rod approximation tilt (θ_{X-ray}) of the molecules in smectic planes was determined using the formula,

$$\theta_{X-ray} = \cos^{-1}(d/l) \tag{2.3}$$

where l is the maximum layer spacing in SmA* phase and d is the layer spacing in the tilted phases. Estimated error in this case is 0.04°.

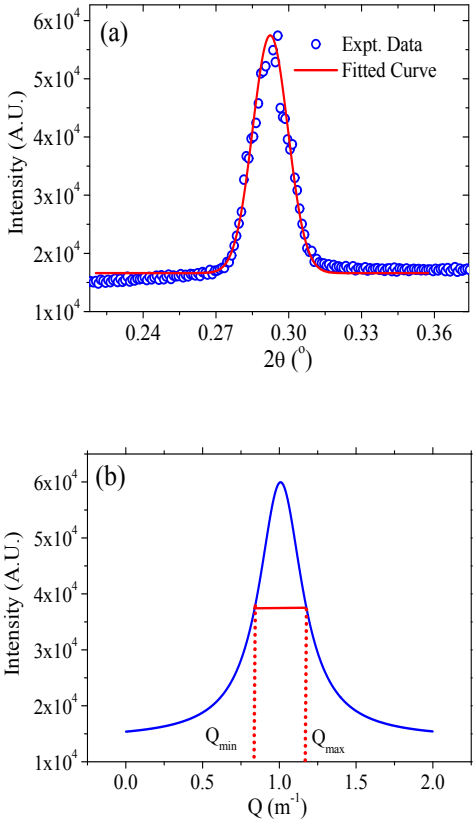

Figure 2.8. (a) Fitted low angle intensity profile, (b) Intensity profile showing FWHM ($\Delta Q = Q_{max} - Q_{min}$)

To probe the extent of correlation of the molecules, correlation lengths (ξ) were calculated both across ($\xi_{\parallel}$) and within ($\xi_{\perp}$) the smectic layers using the following formula.

$$\xi = \frac{2\pi}{\text{FWHM}} = \frac{2\pi}{\Delta Q} \tag{2.4}$$

here FWHM= $\Delta Q = Q_{max} - Q_{min}$, is the full width at half maxima in the scattering vector (Q) of the relevant Bragg peak and was determined from the fitted intensity profile diffraction features (**Figure 2.8**) using Lorentzian fit function of the Origin software.

2.4 DIELECTRIC SPECTROSCOPY

When dielectric materials are placed in an electric field, the electric charges of the molecules shift slightly from their equilibrium position and generate electrical polarization in the material which is called dielectric polarization. Eventually, an internal electric field is produced which reduces the overall electric field within the dielectric. If the dielectric consists of polar molecules, under electric field the molecules orient themselves along the field. The ability of polarization of material in the presence of electric field is different for different materials. Dielectric constant or relative permittivity of a dielectric material is defined as the ratio of the capacitance of a capacitor filled with the material to the capacitance of the same capacitor in vacuum, to measure the ability of polarization of the material. The response of a medium to static electric fields is described by the low-frequency limit of permittivity, also called the static permittivity $\varepsilon(0)$.

$$\varepsilon(0) = \lim_{\omega \to 0} \varepsilon(\omega) \tag{2.5}$$

At the high-frequency limit, the complex permittivity is commonly referred to as $\varepsilon(\infty)$. It is worth pointing out here that for an anisotropic system ε is a tensor with different values in different directions.

The static dielectric permittivity in the uniaxial nematic and smectic-A phases have a tensorial property characterized by two principal components; one component being parallel to director **n** ($\varepsilon_{\parallel}$) and the other being perpendicular to the director **n** ($\varepsilon_{\perp}$). The dielectric anisotropy $\Delta\varepsilon$ in the uniaxial phases is defined as [**34**]

$$\Delta\varepsilon = \varepsilon_{\parallel} - \varepsilon_{\perp} \tag{2.6}$$

When in a dielectric medium an applied field is reversed or withdrawn the polarization of the medium takes a finite time for reorientation. This phenomenon is known as dielectric relaxation. In an alternating field, this leads to a time lag between the field and the reorientation of the polar molecules. As a result, the dielectric permittivity becomes complex and usually expressed as [**35**]

$$\varepsilon^*(\omega) = \varepsilon'(\omega) - i\varepsilon''(\omega) \tag{2.7}$$

here ε' and ε'' are real and imaginary part of ε^*. As long as the molecular reorientation follows the instantaneous field, the induced polarization is constant and the mode is fully contributing to the dielectric permittivity. This constant quantity is

called low frequency permittivity, $\varepsilon'(0)$. At higher frequencies the dipolar reorientations is no longer in phase with the field and the contribution of the mode decreases more and more until it becomes very small. This very small quantity is called high frequency permittivity**,** $\varepsilon'(\infty)$. The difference of these low and high frequency permittivities are defined as dielectric increment or dielectric strength and expressed as

$$\Delta\varepsilon' = \varepsilon'(0) - \varepsilon'(\infty) \tag{2.8}$$

Due to the phase difference between the field (stimulus) and induced polarization (response), a part of the electric energy is dissipated in the form of heat. Thus there is an energy loss (ε'') which is absorbed by the dielectric medium. The energy loss happens to be maximum at a particular frequency, called critical frequency (f_c). It is the reciprocal of the characteristic time of the relaxation**.** There are different dielectric relaxation mechanisms in a dielectric medium, each of which has different origins and are characterized by typical frequency ranges.

2.4.1 DEBYE MODEL

The dielectric permittivity in terms of a single time constant polar substance was described by Debye and is known as Debye model [**36**]. According to this model, the complex dielectric permittivity can be described as

$$\varepsilon^*(\omega) = \varepsilon'(\omega) - i\varepsilon''(\omega) = \varepsilon'(\infty) + \frac{\varepsilon'(0) - \varepsilon'(\infty)}{1 + i\omega\tau} = \varepsilon'(\infty) + \frac{\Delta\varepsilon'}{1 + i\omega\tau} \tag{2.9}$$

This is known as the Debye equation. Relaxation time τ is related to the relaxation frequency (f_c) by the relation

$$\tau = \frac{1}{2\pi f_c} \tag{2.10}$$

The real part (ε') and imaginary part (ε'') of the dielectric permittivity are expressed as

$$\varepsilon'(\omega) = \varepsilon'(\infty) + \frac{\Delta\varepsilon'}{1 + \omega^2\tau^2} \tag{2.11}$$

$$\varepsilon''(\omega) = \frac{\omega\tau\Delta\varepsilon'}{1 + \omega^2\tau^2} \tag{2.12}$$

ε'' reaches its maximum value at critical frequency given by $\omega_c\tau = 1$, and the maximum value is

$$\varepsilon''_{max} = \frac{\Delta\varepsilon'}{2} \tag{2.13}$$

So the maximum value of absorption is just half of the dielectric increment.

The frequency dependence (in logarithmic scale) of ε' and ε'' are shown in **Figure 2.9.** The frequency dependence of ε' is known as dielectric dispersion and the frequency dependence of ε'' is known as dielectric absorption [**37**].

Cole and Cole [**38-39**] showed that in a material exhibiting Debye relaxation the dielectric spectra can also be represented by plotting ε' versus ε'' in a complex plane and the curve obtained is a semicircle with its center lying on ε' axis at $(\varepsilon'(0) + \varepsilon'(\infty))/2$ with radius $(\varepsilon'(0) - \varepsilon'(\infty))/2$. Each point on the semicircle corresponds to the complex dielectric permittivity of the material for a particular frequency (**Figure 2.10**). The Debye equation can be represented as

$$\left(\varepsilon' - \frac{\varepsilon'(0) + \varepsilon'(\infty)}{2}\right)^2 + (\varepsilon'')^2 = \left(\frac{\varepsilon'(0) - \varepsilon'(\infty)}{2}\right)^2 \tag{2.14}$$

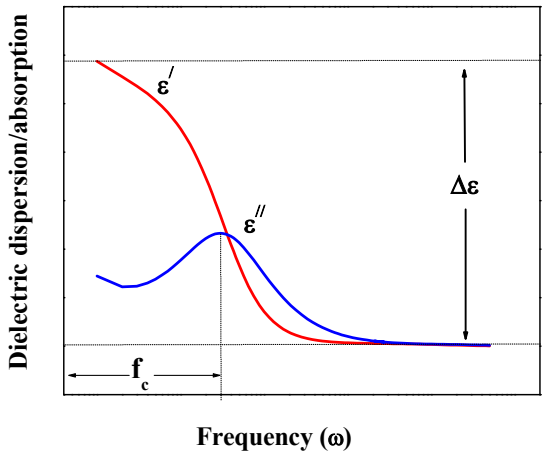

Figure 2.9. Frequency dependence of $\varepsilon'(\omega)$ and $\varepsilon''(\omega)$ for a relaxation process.

This graphical representation of **equation 2.14** is called the Cole-Cole plot. The plot is very useful for checking whether the values of ε' and ε'' are described by a single relaxation time or not, i.e., the plot is showing single semi-circle or multiple semi-circle. Each semi-circle represents a relaxation process.

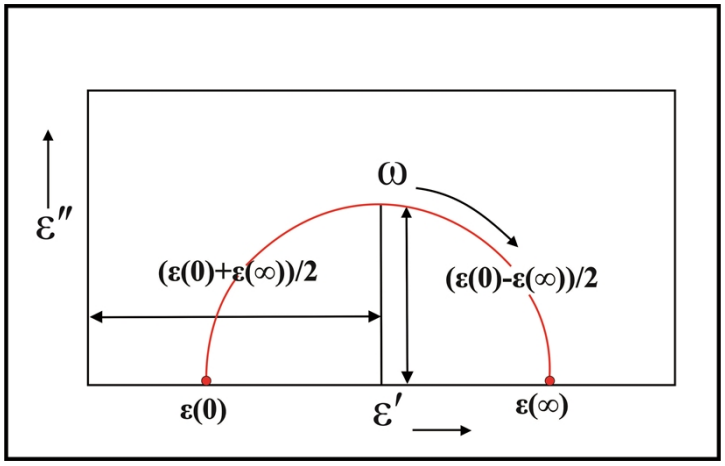

Figure 2.10. Cole-Cole plot of a spectrum showing Debye type relaxation.

2.4.2 COLE-COLE MODEL

For liquid and solid rotator phases of organic polar compounds, the dielectric spectrum is Debye type [**40-41**]. However, in order to describe the dielectric behaviour in some system composed of flexible molecules [**41-44**] and some disordered solid phases [**45-46**] which exhibit broad dielectric spectra, Cole and Cole [**38**] extended the Debye equation by assuming a symmetrical distribution of relaxation times characterized by the symmetry parameter α as follows.

$$\varepsilon^*(\omega) = \varepsilon'(\omega) - i\varepsilon''(\omega) = \varepsilon(\infty) + \sum_k \frac{\Delta\varepsilon'_k}{1 + (i\omega\tau_k)^{1-\alpha_k}} - i\frac{\sigma}{\omega\epsilon_0} \qquad (2.15)$$

symmetry parameter α varies from 0 to 1, here $\Delta\varepsilon'_k = \varepsilon'(0) - \varepsilon'(\infty)$ is dielectric increment, τ_k is relaxation time, and α_k is symmetry parameter signifying deviation from Debye type behaviour of *k*–th mode relaxation process, τ_k is the most probable relaxation time related to critical frequency ω_c and ϵ_0(=8.85pF/m) is the permittivity of the free space. We added the conductivity term in the original Cole-Cole equation in order to consider the effect of conductivity of the cell that arises due to charge impurities and contributes mainly to the low frequency region [**47**]. The real ε′ and imaginary ε″ parts can be expressed as

$$\varepsilon'(\omega) = \varepsilon(\infty) + \Delta\varepsilon' \frac{1 + (\omega\tau_k)^{1-\alpha_k}\sin\left(\frac{1}{2}\pi\alpha\right)}{1 + 2(\omega\tau_k)^{1-\alpha_k}\sin\left(\frac{1}{2}\pi\alpha\right) + (\omega\tau_k)^{2(1-\alpha_k)}} \qquad (2.16)$$

$$\varepsilon''(\omega) = \Delta\varepsilon' \frac{(\omega\tau_k)^{1-\alpha_k}\cos\left(\frac{1}{2}\pi\alpha\right)}{1 + 2(\omega\tau_k)^{1-\alpha_k}\sin\left(\frac{1}{2}\pi\alpha\right) + (\omega\tau_k)^{2(1-\alpha_k)}} + \frac{\sigma}{\omega\epsilon_0} \qquad (2.17)$$

The maximum value of absorption $\varepsilon''_{max}(\omega_c)$ corresponds to a particular frequency; called critical frequency $\omega_c\,(=2\pi f_c)$ and depends on the parameter α according to the formula:

$$\varepsilon''(\omega_c) = \varepsilon''_{max} = \frac{\Delta\varepsilon'}{2}\frac{\cos\left(\frac{1}{2}\pi\alpha\right)}{1+\sin\left(\frac{1}{2}\pi\alpha\right)} \qquad (2.18)$$

For small values of α ($\alpha < 0.1$) the above expression for maximum absorption reduces to

$$\varepsilon''_{max} = \frac{\Delta\varepsilon'}{2+\alpha\pi} \qquad (2.19)$$

Obviously, for dielectric medium which does not obey the Debye type spectrum, the maximum absorption peak in the Cole-Cole plot is lowered and the broadened.

Another general function was proposed by Havriliak and Negami which was an empirical modification of the Debye relaxation model, accounting for the asymmetry and broadness of the dielectric dispersion curve [**48-49**]. The model was first used to describe the dielectric relaxation of some polymers, some disordered solids and also FLCs and AFLCs [**50-52**].

2.4.3 DIELECTRIC RELAXATIONS IN FERROELECTRIC AND ANTIFERROELECTRIC LIQUID CRYSTALS

Before we discuss the relaxation mechanisms in chiral smectic systems, we want to mention here that the time-dependent measuring electric fields are applied to the molecules of smectic layers in two geometries. If the electric field is applied in a direction parallel to the smectic layers i.e., in a direction perpendicular to the molecular director, then transverse component of the permittivity ($\varepsilon_\perp$) is measured and the geometry is known as homogeneous or planar geometry and when the electric field is applied perpendicular to the smectic layers, i.e., in a direction parallel to the

molecular director, then parallel component of the permittivity ($\varepsilon_{\parallel}$) is measured and the geometry is known as homeotropic geometry as shown in **Figure 2.11**. By proper surface treatment of the inner surfaces of the ITO coated glass plates, used to construct the dielectric cell, one may get the homogeneous or homeotropic alignment of the molecules. As in the present dissertation, the dielectric measurements are made in a planar geometry, hence by the term 'dielectric permittivity' we shall mean the transverse component.

The relaxations of dielectric materials are categorized as (i) non-collective relaxations (single molecular), arise from molecular rotation around the short axis, rotation around long axis, intramolecular rotations around single bond and motions of electrons relative to their nuclei and (ii) collective relaxations, arise from the collective reorientations of molecular directors.

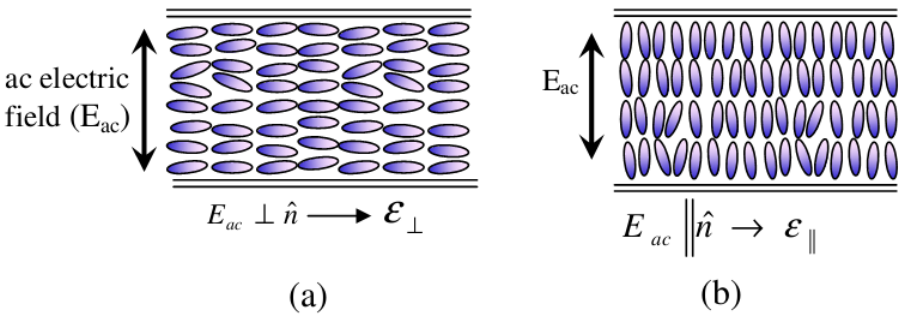

Figure 2.11. (a) Homogeneous arrangement of molecules and transverse component of the permittivity ($\varepsilon_{\perp}$) (b) homeotropic arrangement of molecules and parallel component of the permittivity ($\varepsilon_{\parallel}$).

The dielectric response of ferroelectric system exhibiting SmC* and SmA* phase consists of four modes of relaxations two of which are (i) Goldstone mode (GM) and (ii) soft mode**,** related to the collective director fluctuations, lie in a few tens Hz to a few hundred kHz ranges. The other two modes are non-collective (molecular), related to the fluctuation of polarization and observed in the frequency range of several hundred kHz to a few GHz. It is not usually visible by dielectric spectroscopy when the planar orientation of the molecules exists in the measuring cell. We have investigated the collective relaxations only.

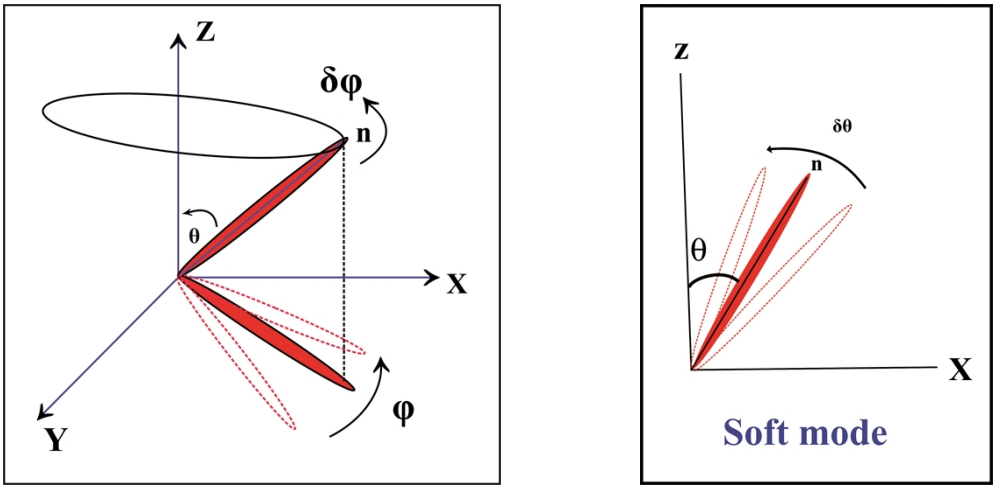

(a) (b)

Figure 2.12. Schematic representation of director fluctuation in (a) the Goldstone mode relaxation, originates from the phase fluctuation ($\delta\varphi$) of the director in chiral SmC* phase, (b) the soft mode relaxation, arises due to the tilt ($\delta\theta$) fluctuation of the molecular director.

Goldstone mode is observed in SmC* phase and arises from the phase fluctuation of azimuthal orientation of the director [**35, 53-55**] and hence also called as a phason mode. Its amplitude is high and hence the dielectric increment is also high and corresponding relaxation frequency is low. The Goldstone mode relaxation frequency and dielectric increment have only weak temperature dependence [**35**, **56**].

The soft mode arises from the tilt fluctuation of the director in SmA* phase and within SmC* phase but near the SmA*-SmC* transition [**35, 55, 57**]. This is also called amplitude mode. Although the dielectric increment of soft mode is much lower than the Goldstone mode, the soft mode critical frequency is at least two orders higher than that of GM. In SmC* phase, the weak SM dielectric spectra are usually masked by the strong Goldstone dielectric spectra hence it creates difficulty to explore the SM unless the GM is suppressed applying DC bias field.

From Landau model the concept of soft mode was first introduced to the SmA*–SmC* phase transition by Blinc and Zeks [**57**] for the case of a modulated structure and later modified by Carlsson *et al.* [**56**] where phase transition is described in terms of two order parameters – two-component tilt vector as primary order parameter and two-component in-plane polarization as the secondary order parameter. Two characteristic modes are observed in SmA*–SmC* second order phase transition

where the continuous symmetry group of SmA* (D_∞) is spontaneously broken in SmC*(C_2). The soft mode is a symmetry breaking mode, which critically slows down (softens) on approaching the phase transition from above, the Goldstone mode is zero frequency mode that tries to restore the broken symmetry. Thus soft mode splits into the phason (GM) and amplitude (SM) modes in SmC* near the transition.

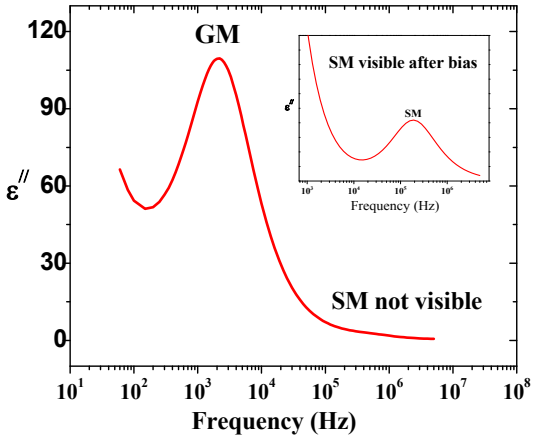

Figure 2.13. Goldstone mode and soft mode in a frequency window, the soft mode becomes prominent after the Goldstone mode is suppressed under DC bias (inset).

Under a strong bias field in SmC* phase a residual mode, with dielectric spectrum different from that of GM, is observed, this mode is known as domain mode (DM) [**58-60**]. Beresnev *et al*. [**61**] discovered that ferroelectric liquid crystals with high spontaneous polarization can form solid ferroelectric like domain after suppression of GM; the relaxation mode arising out of such domain is termed as domain mode. Haase *et al*. [**62**] gave the same argument regarding the arising of the domain mode.

In the antiferroelectric phase two collective relaxation processes are usually observed – one in low frequency region (few hundred Hz to few kHz), called in-phase antiferroelectric (P_L) mode and the other, comparatively in higher frequency region (few kHz to few hundred kHz ranges), is called anti-phase antiferroelectric (P_H) mode [**63-68**]. Typical absorption spectra are shown in **Fig. 2.14**.

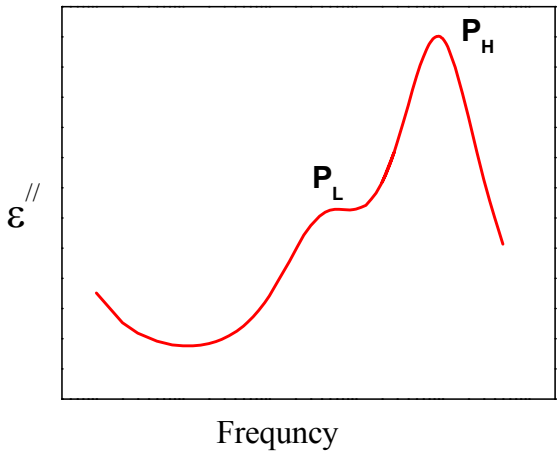

Figure 2.14. The absorption spectrum in SmC_A^* phase showing P_L and P_H mode.

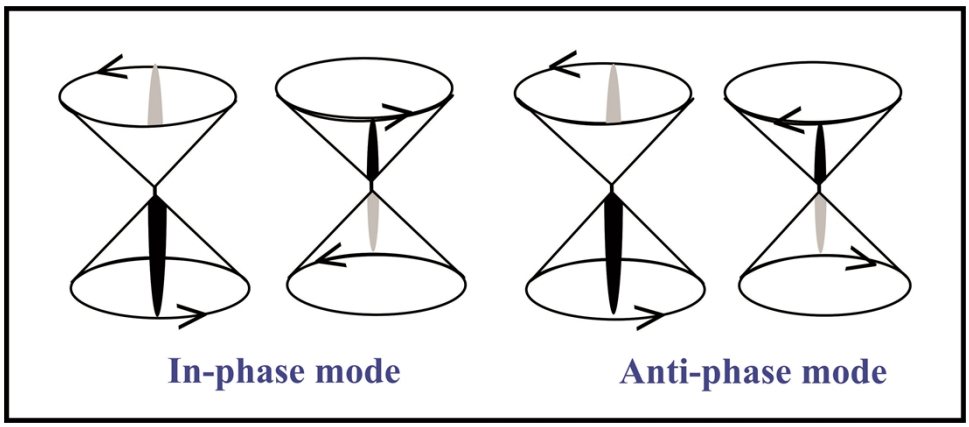

Figure 2.15. Schematic representation of molecular rotations in successive layers in the in-phase P_L and the anti-phase P_H mode [**69**].

Diverse reports on range and temperature dependence of critical frequencies of both the modes are found in literature. J. Hou *et al.* [**63**] first reported that the modes P_L and P_H might arise due to in-phase and anti-phase fluctuation of molecules in the adjacent smectic layers (**Fig. 2.15**). Although there is ambiguity regarding the origin of the two modes, a strong correlation of bias dependence of absorption strengths of P_L and P_H modes indicates that their origin should be correlated.

2.4.4 DIELECTRIC MEASUREMENT TECHNIQUE

The dielectric behavior of liquid crystalline material is studied by measuring the complex dielectric permittivity at constant temperature and ambient pressure within a frequency domain and is commonly known as frequency domain dielectric spectroscopy (FDDS). The FDDS may be performed at varying temperatures during heating as well as cooling. The peaks in the absorption spectrum represent a dielectric relaxation. Examining the range of critical frequencies, absorption peak heights, and its behavior under bias one may decide about the relaxation mode and may decide about the phase in which it is arising. To find the dielectric increment, relaxation frequency and symmetry parameter of a particular mode, dielectric absorption spectra were fitted by non-linear least squares method to **equations 2.16** and **2.17.** In most cases, we had to fit two relaxation processes.

In the present work dielectric studies were performed using Indium-Tin oxide (ITO) coated homogeneously (HG) aligned EHC cells of thickness 10 μm (5 μm was used to study the nanocomposite). The sheet resistance of the ITO coated glass was low (20 Ω per sheet is used). This is because, at high frequencies, the effect of ITO resistance is seen as an increase in dielectric absorption and a decrease in dielectric permittivity, which mimics a relaxation process in the dielectric spectrum. The overlapping active area of the cell is 1.0 cm^2. Dielectric measurements were made using HIOKI 3532-50 impedance analyzer (40 Hz – 5 MHz), cell temperature was controlled within ± 0.1^oC placing the cell inside the Mettler FP82 hot stage. An automatic data acquisition arrangement was made using RS 232 interface with a PC. The experimental set up is shown in **Figure 2.16**.

The real and imaginary parts of the dielectric permittivity at a frequency were obtained as follows

$$\varepsilon'(\omega) = \frac{C}{C_o} \text{ and } \varepsilon''(\omega) = \varepsilon'(\omega)\, tan\delta \qquad (2.20)$$

where C is the capacitance of the cell filled with LC and C_o is that of the empty cell and $tan\delta$ is the dielectric loss. The effect of stray capacitances was eliminated by standard process.

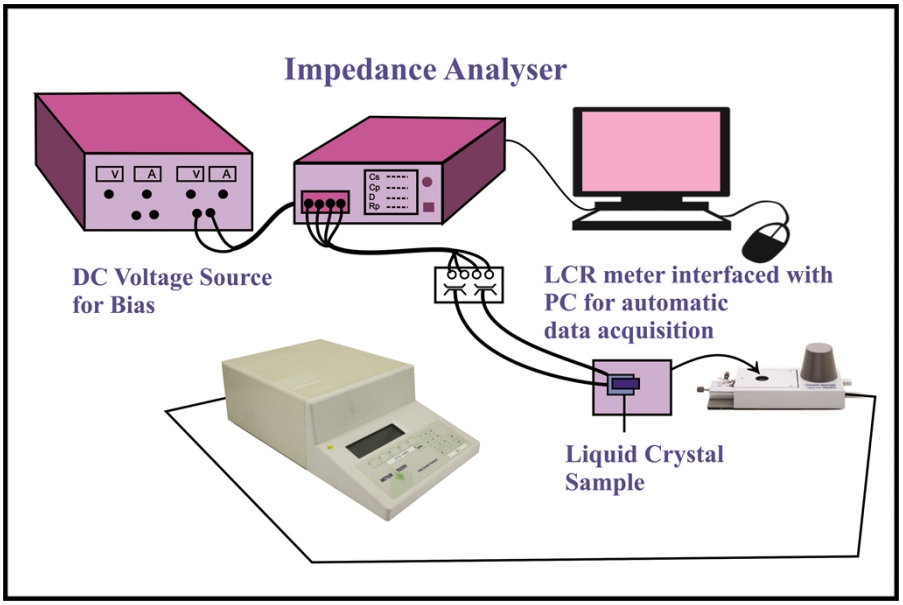

Figure 2.16. Experimental set up for dielectric spectroscopy.

There are two main sources of symmetric errors in the quantitative evaluation of the dielectric permittivity. One source is in the high frequency region due to the resistance of the ITO conducting layer. The ITO resistances were kept below 20Ω in order to reduce the high frequency effect. Moreover, our dielectric measurements are within the frequency window of 5MHz, hence there is a little possibility of arising error due to high frequency effect. The other source of error is in the low frequency region due to the freely moving ions and contribution from the dipolar reorientation. The measured data were fitted to suitable functions and the correct results were extracted. The accuracy in the measurement of capacitance (C) and tanδ (G) in the frequency range is <0.2% and hence maximum uncertainty in the measurement of dielectric permittivity (ε') and dielectric loss (ε'') within entire frequency regime is less than ±1%.

2.5 MEASUREMENTS OF ELECTRO-OPTIC PARAMETERS – TILT ANGLE (θ), SPONTANEOUS POLARIZATION (P_s), THE SWITCHING TIME (τ) AND ROTATIONAL VISCOSITY (γ_φ)

The spontaneous polarization in SmC* phase would feel a torque (**P**×**E**) in an electric field and it is a linear effect, although the other liquid crystals show an electrooptic effect with a response quadratic in the field, i.e. not sensitive to the sign

of E. The linear effect was verified by R. B. Meyer **[70].** The transition from SmA*-SmC* is typically 2nd order, which implies that the tilt angle θ increases with temperature as $\theta \sim (T_c - T)^{1/2}$ [**71**], where T_c is transition temperature and T is any temperature below T_c (**Figure 2.17**). As the Ps ought to be essentially proportional to the tilt, it could be expected to increase in the same way, which was also proved in subsequent measurements.

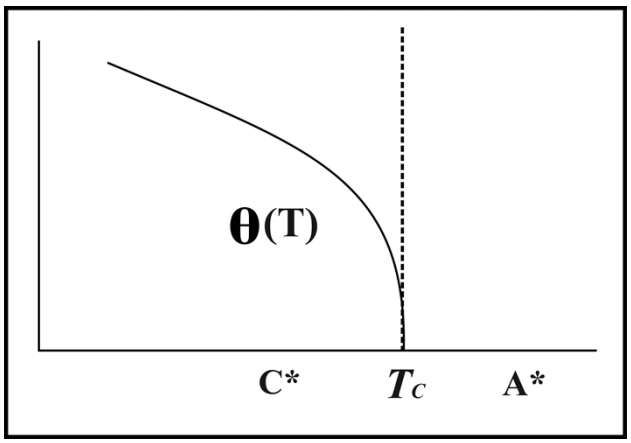

Figure 2.17. The molecular tilt θ as a function of temperature near the SmA*−SmC* transition [**71**].

By applying an electric field (*E*) across a thin transparent cell one can induce a rotation of the molecular axis in the plane of the cell. On reversing the field the molecules rotate by twice the conic angle θ (2θ). This molecular motion is called electrooptic switching which occurs in a viscous medium with a characteristic time τ,

$$\tau = \frac{\gamma_\varphi}{P_s E} \tag{2.21}$$

here γ_φ is rotational viscosity, P_s is spontaneous polarization [**72**]. With a moderate value of P_s, the low-viscous compounds will help to achieve sub-microsecond switching.

2.5.1 TILT ANGLE (θ)

The molecular tilt angle θ, the angle made by the molecular long axis with the layer normal, is considered as the primary order parameter of ferroelectric and antiferroelectric liquid crystals. To measure the molecular tilt (θ), a pulse electro-optical technique was proposed by Baikalov *et al.* [**73**] based on the linear electro-optical effect. In an ac field, the chiral molecules switch around an imaginary cone

through twice the tilt angle θ (2θ) thereby reversing the sign of spontaneous polarization. The ferroelectric or antiferroelectric sample is taken in a capacitive cell in planar arrangement (same cell as in dielectric measurements). The cell is taken on the turntable of the polarizing microscope with crossed polarizers and polarized light is passed normally through glass plates of the cell. An electric field of sufficiently high magnitude is applied so that the helix is unwound and the molecules are aligned uniformly with a tilt θ away from the layer normal. The sample cell is rotated to get the minimum optical transmission. Then the field is reversed and the sample cell is rotated in the opposite direction to achieve again the minimum transmission. The difference in angular readings on the microscope turntable for two nearby transmission minima gives twice the tilt angle (2θ) [**73-74**]. In our experiments about 20V (Vpp) square wave pulses of low frequency (about 50 mHz) were used. Estimated error in the tilt measurement was 0.2°.

2.5.2 SPONTANEOUS POLARIZATION (P_s)

Chiral smectic liquid crystals in surface stabilized geometry possess permanent dipoles normal to their molecular axis which gives rise to existence of polarization even in absence of an external field and is called spontaneous polarization (P_S). Ps is the result of tilt (θ) of the molecules, and is essentially proportional to the θ, and is considered as secondary order parameter.

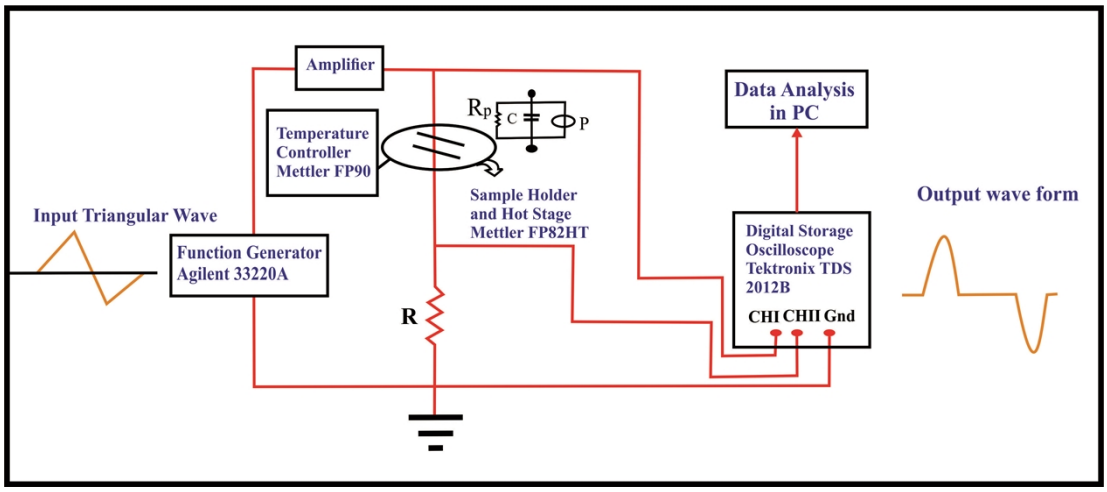

Figure 2.18. Block diagram of the experimental set up for the measurement for electro-optic parameters (P_s, τ, θ, etc.).

There are several methods to measure the Ps of ferroelectric materials. But a comparison of Ps values of DOBAMBC at a particular temperature shows a scattering over one decade and one of the main reason of which, according to K. Miyasto *et al.* [**75**], is the use of different methods.

The standard Sawyer-Tower method [**76**] for the determination of Ps of solid ferroelectric samples was used by several groups for the determination of Ps of ferroelectric liquid crystal [**77-79**]. The electric field dependent dielectric constant method has also been employed [**80**]. The other method is based on the measurement of current induced by rapidly reversing square wave field [**81-82**] in which the main problem was to separate the polarization bump from the baseline of the total current. The most useful technique was introduced by K. Miyasato *et al.* [**75**] utilizing triangular wave, in which the polarization bump can easily be separated from the base line of total current. Assuming the filled LC cell is equivalent to a parallel RC combination, the current induced in the cell due to passing of a triangular wave are composed of three components, namely, the capacitive term $i_c = C(dV/dt)$, the resistive term $i_R = V/R$, (R, the effective resistance of the cell), and the polarization current $i_p = dP/dt$.

$$I = i_c + i_R + i_p = C\frac{dV}{dt} + \frac{V}{R} + \frac{dP}{dt} \tag{2.22}$$

The first two terms exist at all the voltages but i_P appears as hump only when the applied voltage is high enough to unwind the helix and leads to the polarization reversal in the sample.

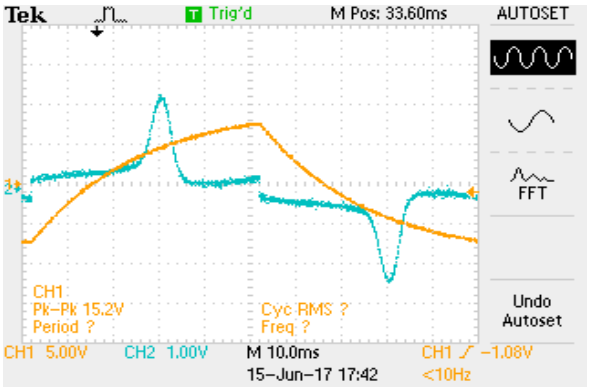

Figure 2.19. The voltage waveform across resistor R, obtained from oscilloscope Tektronics TDS 2012 B in response to the triangular wave.

The voltage drop across a resistance R, connected in series with cell, is stored in a digital oscilloscope (**Fig. 2.19**). R is usually chosen less than the cell resistance R_P so that the time constant for the exponential decay is considerably shorter than the polarization reversal **[83].** Subtracting the ionic and capacitive current, by drawing an appropriate baseline, from the overall voltage profile, the area under the polarization peak is found out which is $\int V(t)dt$. The P_s is calculated from the following formula.

$$P_s = \frac{1}{2AR}\int V(t)dt \tag{2.23}$$

here A is the effective area of the cell. In our experiments, we recorded the voltage waveform across R using a digital storage oscilloscope (Tektronix 2012B). A triangular wave pulse of frequency 10 Hz and varying amplitude from Agilent 33220A LXI function generator was amplified 20 times (F20 Amplifier, FLC, Sweden) and applied across the combination of a standard resistor ($R = 100\ k\Omega$) and the cell containing the sample. The voltage wave across R and the input voltage wave at a fixed temperature were recorded using a digital storage oscilloscope Tektronix 2012 B in separate channels. The area of the polarization hump was calculated after using an appropriate baseline in Origin 8.5 software. The process of estimation of P_s was done at regular temperature intervals both during heating as well as cooling cycle. Estimated error in P_s measurement is less than 1%.

2.5.3 SWITCHING TIME (τ)

The response of a ferroelectric material to a triangular wave is discussed above. The response of the same material to the square wave is shown in **Figure 2.20**. The response of the ions to the field is instantaneous and the current wave (or voltage wave) due to ions follows the applied field instantaneously. But the response of the ferroelectric polarizations are not instantaneous to the applied filed thus the peak due to their reversal occurs over the exponential decay curve of the current wave (or voltage wave) away on the time scale from the square-pulse edge. This delay in time corresponds to the response time of switching between the stable states of polarization and represents the time in which the average number of molecules reorients after applying the pulse [**83**]. Incidentally, this representation of response time from the current signal coincides with the electro-optical transmission from 10% to 90% [**84**]. Estimated error in the measurement of response time is less than 4%.

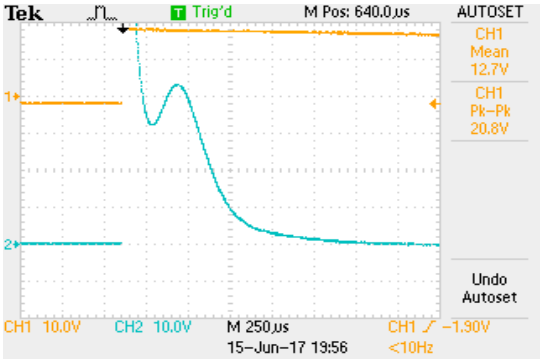

Figure 2.20. The voltage waveform of the response of the ferroelectric liquid crystal to the square pulse wave.

2.5.4 Rotational Viscosity (γ_φ)

Rotational viscosity (γ_φ) is the viscosity associated with the rotation of the molecules about the smectic-C cone and it strongly influences the switching of the molecules between two field-induced states. Measuring P_s and τ, the value of γ_φ was calculated using the relation [**72**]

$$\gamma_\varphi = \tau_s \cdot P \cdot E \tag{2.24}$$

where E is the applied electric field.

Determination Activation Energy (E_a)

If we consider the reorientation of director of molecules of a ferroelectric or antiferroelectric material is a thermally activated process of Arrhenius type [**72, 85**] then the viscosity can be represented as

$$\gamma_\varphi = \gamma_0 e^{\frac{E_a}{k_\beta T}} \tag{2.25}$$

where k_β is Boltzmann constant, γ_0 is pre-exponential term and E_a is the activation energy which according to Arrhenius, the energy for any thermally activated process to start. The above equation signifies that the viscosity will decrease with increasing temperature. Taking the logarithm of both sides,

$$\ln \gamma_\varphi = \left(\frac{E_a}{k_\beta}\right)\frac{1}{T} + \ln \gamma_0 \tag{2.26}$$

Thus from a plot $\ln \gamma_\varphi$ against $(1/T)$, the activation energy can be determined.

2.6 REFERENCES

[1] I. Dierking, Textures of liquid crystals WILEY-VCH, GmbH & Co. KGaA p-16 (2003).

[2] A. Wiegeleben, and D. Demus, Calorimetric Investigations in Liquid Crystalline Terephthalylidene-bis- [4-n-alkylanilines], Crystal Res. & Technol. 17(1982) 161-165.

[3] C. R. Safinya, M. Kaplan, J. Als-Nielsen, R. J. Birgeneau, D. Davidov, J. D. Litster. D.L. Johson, and M.E. Neubert, High-resolution x-ray study of a smectic-A-smectic-C phase transition, Phys. Rev. B. 21(9) (1980) 4149-4153.

[4] P. S. Clegg, X-ray studies of the phases and phase transitions of liquid crystals, Acta Cryst. A61 (2005)112-121.

[5] S. Wrobel, Dielectric Relaxation Spectroscopy, in W. Haase, S. Wrobel (Ed.), Relaxation phenomena – Liquid crystals, magnetic systems, polymers, high–T_C superconductors, metallic glasses, Springer–Verlag, Berlin–Heidelberg, 2003, pp. 13.

[6] G. Vertogen, and W. H. de Jeu (Eds.), Thermotropic Liquid Crysatals Fundamen-tals, Springer-Verlag, (1988), p-207.

[7] G. R. Luckhurst in Liquid Crystals & Plastic Crystals (G. W. Gray and P. A. Winsor, Eds.), Ellis Horwood Limited, 1974, Vol 2, p-144.

[8] C. L. Khetrapal and A. C. Kunwar in Advances in Liquid Crystals, Vol. 1-6, Ed. G. H. Brown, pp-173, Academic Press (1983).

[9] W. J. Borer, S. S. Mitra, and C. W. Brown, Crystal to Liquid-Crystal Transition Studied by Raman Scattering, Phys Rev. Lett. 27(7) (1971) 379-380.

[10] V. D. Neff in Liquid Crystals & Plastic Crystals (Ed. G. W. Gray and P. A. Winsor), Ellis Horwood Limited, Vol 2, p-231 (1974).

[11] S. J. Gupta, R. A. Gharde and A. R. Tripathi, Phase Transition Temperatures of LCs using Fabry-Perot Etalon, Mol. Cryst. Liq. Cryst. 364 (2001) 461- 468.

[12] D. Demus, Textures of liquid crystals, Verlag Chemie Weinheim, New York (1978).

[13] Bouligand in Handbook of Liquid Crystals. Vol. 1 (Fundamentals), Ed. D. Demus, J. Goodby, G. W. Gray, H.-W. Spiess and V. Vill, WILEY-VCH, Verlag GmbH, Weinheim, FRG (1998), Defects and textures.

[14] A. J. Slaney, K. Takatohi and J. W. Goodby in The Optics of Thermotropic Liquid Crystals, Ed. S. Elston and R. Sambles, Taylor & Francis (1998), Defect textures in liquid crystals.

[15] G.W.H. Hohne, W. Hemminger, H. J. Flammersheim, Differential Scanning Calorimetry, An Introduction for Practitioners, Springer (1994).

[16] D. Mazotko and D. Demus, Advances in Liquid Crystals, Pramana Suppl. 1 (1976) 189.

[17] A. Wiegeleben and D. Demus, Calorimetric Investigations in Liquid Crystalline Terephthalylidene-bis- [4-n-alkylanilines], Crystal Res. & Technol. 17 (1982) 161-165 (TBAA).

[18] B. K. Vainstein, Diffraction of X-rays by Chain Molecules, Elsevier, Amsterdam (1966).

[19] H. Kelkar and R. Hatz, Handbook of Liquid Crystals, Verlag Chemie, Ch.5 (1980).

[20] P. S. Pershan, Structure of Liquid Crystalline Phases, World Scientific, Singapore (1988).

[21] G. Ungar in Physical properties of liquid crystals, D. A. Dunmur, A. Fukuda and G. R. Luckhurst (Eds.), INSPEC, London, Ch. 4.1 (2001).

[22] B. Jha, S. Paul, R. Paul and P. Mandal, Order parameters of some homologue cybotactic nematics from X-ray diffraction measurements, Phase Transit. 15 (1989) 39-48.

[23] S. Diele, P. Brand and H. Sackmann, X-ray Diffraction and Polymorphism of Smectic Liquid Crystals 1. A-, B- and C-modifications, Mol. Cryst. Liq. Cryst. 16 (1972) 105-116.

[24] A. de Vries, X-Ray Studies of Liquid Crystals: V, Classification of Thermotropic Liquid Crystals and Discussion of Intermolecular Distances, Pramana Suppl. No.1 (1975) 93.

[25] A. de Vries, A. Ekachai and N. Spielberg, X-Ray Studies of Liquid Crystals VI The Structure of the Smectic A, C, Bn and Bt Phases of Trans-1, 4-Cyclohexane-DI-N-Octyloxybenzoate. J. de Phys. Collques. 40(C3) (1979) C3-147-C3-152.

[26] A. J. Lead better, J. Prost, J. P. Gaughan and M. A. Mazid, The structure of the crystal, SmE and SmB forms of IBPBAC. J. de Phys. Colloques. 40 (1979) C3-185 – C3-193.

[27] A. J. Leadbetter and P. G. Wrighton, Order parameters in S_A, S_C and N phases by X-ray diffraction, J. de Phys. 40 (1979) C3-234 – C3-242.

[28] V. M. Sethna, A. de Vries and N. Spielberg, X-Ray Studies of Liquid Crystals VIII: A Study of the Temperature Dependence of the Directly Observed Parameters of the Skewed Cybotactic Nematic Phase of Some Bis-(4′-n-Alkoxybenzal) -2-Chloro-1,4-Phenylenediamines, Mol. Cryst. Liq. Cryst. 62 (1980)141-153.

[29] L. V. Azaroff and C. A. Schuman, X-Ray Diffraction by Cybotactic Nematics, Mol. Cryst. Liq. Cryst. 122 (1985) 309-319.

[30] A. de Vries, The Use of X-Ray Diffraction in the Study of Thermotropic Liquid Crystals with Rod-Like Molecules, Mol. Cryst. Liq. Cryst. 131(1985) 125-145.

[31] P. Mandal, M. Mitra, S. Paul and R. Paul, X-Ray Diffraction and Optical Studies of an Oriented Schiff‘s Base Liquid Crystal, Liq. Cryst. 2 (1987) 183-193.

[32] A. de Vries, X-ray Photographic Studies of Liquid Crystals I. A Cybotactic Nematic Phase, Mol. Cryst. Liq. Cryst. 10(1970) 219-236

[33] H. F. Gleeson and L. S. Hirst, Resonant X-ray Scattering: A Tool for Structure Elucidation in Liquid Crystals, Chem. Phys. Chem. 7 (2006) 321 – 328.

[34] F. M. Gouda, Dielectric relaxation spectroscopy of chiral smectic liquid crystals, Ph. D. thesis, Department of Physics, Chalmers University of Technology, Goteborg, Sweden (1992).

[35] F. Gouda, K. Skarp, and S.T. Lagerwall, Dielectric studies of the soft mode and goldstone mode in ferroelectric liquid crystals, Ferroelectrics. 113 (1991) 165-206.

[36] P. Debye, Polar Molecules. Dover publications, New York, USA (1929).

[37] S. Haldar, Investigation on some achiral and chiral mesogenic systems by different experimental techniques. Ph. D. Thesis (2013), University of North Bengal, Siliguri, India.

[38] K. S. Cole and R. H. Cole, Dispersion and Absorption in Dielectrics I. Alternating Current Characteristics**,** J. Chem. Phys. 9 (1941) 341.

[39] K. S. Cole and R. H. Cole, Dispersion and Absorption in Dielectrics II. Direct Current Characteristics, J. Chem. Phys. 10 (1942) 98.

[40] C. J. F. Bottcher, and P. Bordewijk, Ed., Theory of Electric Polarization, Vol II. Dielectric in time-dependent fields, Elsevier, Scientific Publishing Co. (1973).

[41] N. Hill, W. E. Vaughan, A. H. Price, and M. Davies, Dielectric Properties and Molecular Behavior, Van Nostrand, London (1969).

[42] W. Haase, H. Pranoto, F. J. Bormnuth, B. Bunsenges, Dielectric Properties of Some Side Chain Liquid Crystalline Polymers, Phys. Chem., 89 (1985) 1229-1234.

[43] C. P. Smyth, Dielectric Behavior and Structure, pp. 441. McGraw-Hill, N.Y. (1955).

[44] V. I. Minkin, O. A. Osipov, and Y. A. Zhdanov, W.E. Vaughan, Dipole Moments and the Electronic Structure of Organic Compounds. In: Vaughan W.E.(eds) Dipole Moments in Organic Chemistry, Springer Link, New York-London (1970).

[45] A. K. Jonscher, Dielectric Relaxation in Solids, Chelsea Dielectric Press, London (1983).

[46] S. Wrobel, B. T. Gowda, and W. Haase, Dielectric study of phase transitions in 3-nitro-4-chloro-aniline, J. Chem. Phys 106 (10) (1997) 5904-5409.

[47] W. Haase, S. Wrobel (Ed.), Relaxation phenomena – Liquid crystals, magnetic systems, polymers, high–T_C superconductors, metallic glasses, Springer–Verlag, Berlin–Heidelberg, 2003, pp. 20.

[48] S. Havriliak, and A. Negami, Complex plane analysis of α-dispersions in some polymer systems, S. J. Polimer Sci. C. 14 (1966) 99-117.

[49] S. Havriliak, and A. Negami, complex plane representation of dielectric and mechanical relaxation processes in some polymers, S. J. Polimer Sci. 8 (1967) 161-210.

[50] D. Ganzke, S. Wrobel, and W. Haase, Dielectric studies of bicyclohexylcarbonitrile nematogens with large negative dielectric anisotropy, Mol. Cryst. Liq. Cryst. 409 (2004) 323-333.

[51] H. Uehara, Y. Hanakai, J. Hatano, S. Saito, and K. Murashiro, Dielectric Relaxation Modes in the Phases of Antiferroelectric Liquid Crystals, Jpn. J. Appl. Phys. 34 (1995) 5424-5428.

[52] A. Fafara, B. Gestblom, S. Wrobel, R. Dabrowski, W. Drzewinski, D. Kilian, and W. Haase, Dielectric spectroscopy and electrooptic studies of new MHPOBC analogues, Ferroelectrics. 212 (1998) 79-90.

[53] A. M. Biradar, S. Wrobel and W. Haase, Dielectric relaxation in the smectic-A^* and smectic-C^* phases of a ferroelectric liquid crystal, Phys. Rev. A. 39 (1989) 2693-2702.

[54] J. K. Ahuja, and K. K. Raina, Polarization Switching and Dielectric Relaxations in Ferroelectric Liquid Crystals, Jpn. J. Appl. Phys. 39 (2000) 4076-4081.

[55] Y. P. Panarin, O. Kalinovskaya, J. K. Vij, and J. W. Goodby, Observation and investigation of the ferrielectric subphase with high q_T parameter, Phys. Rev.E. 55 (1997) 4345-4353.

[56] T. Carlsson, B. Zeks, C. Filipic and A. Levstik, Theoretical model of the frequency and temperature dependence of the complex dielectric constant of

ferroelectric liquid crystals near the smectic-C*- smectic- A* phase transition, Phys. Rev.A. 42 (1990) 877-889.

[57] R. Blinc and B. Zeks, Dynamics of helicoidal ferroelectric smectic-C^* liquid crystals, Phys. Rev. A. 18 (1978) 740-745.

[58] J. M. Czerwiec, R. Dabrowski, K. Garbat, M. Marzec, M. Tykarska, A. Wawrzyniak, S. Wrobel, Dielectric and electro-optic behaviour of two chiral compounds and their antiferroelectric mixtures, Liq. Cryst. 39(12) (2012) 1503-1511.

[59] M. Marzec, W. Haase, E. Jacob, M. Pfeiffer, S. Wrobel, The existence of four dielectric modes in the planar oriented S^*_c phase of a fluorinated substance, Liq. Cryst. 14 (2) (1993) 1967-1976.

[60] S. Wrobel, G. Cohen, D. Davidov, W. Hasse, M. Marzec, M. Pfeiffer, Dielectric, electro optic and X-ray studies of a room temperature ferroelectric mixture, Ferroelectrics. 166 (1995) 211-222.

[61] L. A. Beresnev, M. V. Loseva, N. I. Chernova, S. G. Kononov, P. V. Adomenas, E. P. Pozhidayev, Pis'ma Zh. Eksp. Teor. Fiz. 51 (1990) 457.

[62] W. Haase, S. Hiller, M. Pfeiffer, L. A. Beresnev, The domain mode in ferroelectric liquid crystals; electrooptical and dielectric investigations, Ferroelectrics. 140 (1993) 37-44.

[63] J. Hou, J. Schacht, F. Giebelmann and P. Zugenmaier, Temperature and bias-field dependences of dielectric behaviour in the antiferroelectric liquid crystal, (R)-MHPOBC, Liq. Cryst. 22(4) (1997) 409-417.

[64] M. Buivydas, F. Gouda, G. Andersson, S.T. Lagerwall, B. Stebler, Collective and non-collective excitations in antiferroelectric and ferrielectric liquid crystals studied by dielectric relaxation spectroscopy and electro-optic measurements, Liq. Cryst. 23(5) (1997) 723-739.

[65] Yu. Panarin, O. Kalinovskaya, and J. K. Vij, The investigation of the relaxation processes in antiferroelectric liquid crystals by broad band dielectric and electro-optic spectroscopy, Liq. Cryst. 25 (2) (1998) 241-252.

[66] Y. P. Panarin, O. Kalinovskaya, J. K. Vij, The relaxation processes in helical antiferroelectric liquid crystals, Ferroelectrics. 213 (1998) 101-108.

[67] P. Perkowski, K. Ogrodnik, W. Piecek, M. Zurowska, Z. Raszewski, R. Dabrowski, L. Jaroszewicz, Influence of the bias field on dielectric properties of the SmC_A* in the vicinity of the SmC*–SmC_A* phase transition, Liq. Cryst. 38(16) (2011) 1159-1167.

[68] Yu. Panarin, O. Kalinovskaya, and J. K. Vij, Observation and investigation of the ferroelectric subphases with high q_T parameter, Phy. Rev. E. 55(4) (1997) 4345-4353.

[69] M. Baral, A. P. Ranjitha and S. Krishna Prasad, Confinement of an antiferroelectric liquid crystal in a polymer nanonetwork: thermal and dielectric behavior, Bull. Mater. Sci. 41 (2018) 135 (1-7).

[70] R. B. Meyer, L. Liebert, L. Strzelecki, P. Keller, Ferroelectric liquid crystals, Journal de Physique Lettres, Edp sciences, 1975 36 (3) 69-71.

[71] S. T. Lagerwall, Ferroelectric and Antiferroelectric Liquid Crystals. Ferroelectrics. 301 (2004) 15–45.

[72] S. T. Lagerwall, B. Otterholm and K. Skarp, Material properties of ferroelectric liquid crystals and their relevance for applications and devices, Mol. Cryst. Liq. Cryst. 150 (1987) 503-587.

[73] V. A. Baikalov, L. A. Beresnev and L. M. Blinov, Measures of the Molecular Tilt Angle and Optical Anisotropy in Ferroelectric Liquid Crystals, Mol. Cryst. Liq. Cryst. 127 (1985) 397-406.

[74] M. Buivydas, P. Adomenas, S. T. LAgerwall and B. Stebler, The Spontaneous Polarisation and Rotational viscosity in Host-dopant Mixtures, Ferroelectrics. 166 (1995) 165-174.

[75] K. Miyasato, S. Abe, H. Takezoe, A. Fukuda and E. Kuze, Direct Method with Triangular Waves for Measuring Spontaneous Polarization in Ferroelectric Liquid Crystals, Jpn. J. Appl. Phys. 22 (10) (1983) L661-L663.

[76] C. B. Sawyer and C. H. Tower, Rochelle salt as a Dielectric, Phys. Rev. 35 (1930) 269-273.

[77] H. Mstsuma, The Ferroelectricity in the Mixtures of Chiral with Non-Chiral Smectic C, Mol. Cryst. Liq. Cryst. 49 (1978)105-112.

[78] B. I. Ostrovski, A. Z. Rabinovich, A. S. Sonin, E. L. Sorking, B. A. Strukov and S.A. Taraskin, Ferroelectric behaviour of different classes of smectic liquid crystal, Ferroelectrics. 24 (1980) 309-312.

[79] M. Imasaki, T Fujimoto, T Nishihara, T. Yoshioka and Y. Narushige, Ferroelectricity in Mixtures of Chiral Smectic C and Smectic A Liquid Crystals, Jpn. J. Appl. Phys. 21 (1982) 1100-1100.

[80] T. Uemoto, K. Yoshino and Y. Inuishi, Ferroelectric Properties of Chiral Smectic Liquid Crystal, Jpn. J.Appl. Phys. 18(7) (1979) 1261-1265.

[81] M. Buivydas, P. Adomenas, S. T. Lagerwall and B. Stebler, The Spontaneous Polarisation and Rotational viscosity in Host-dopant Mixtures, Ferroelectrics. 166 (1995) 165-174.

[82] I. Dahl, S. T. Lagerwall and K. Skarp, Simple model for the polarization reversal current in a ferroelectric liquid crystal. Phys. Rev. A. 36(9) (1987) 4380-4390.

[83] K. Skarp, I. Dahl, S.T. Lagerwall and B. Stebler, Polarisation and viscosity measurements in a ferroelectric liquid crystal by the field reversal method, Mol. Cryst. Liq. Cryst. 114 (1984) 283-297.

[84] S. S. Bawa, A. M. Biradar, K. Saxena and S. Chandra, Direct pulse technique for spontaneous polarization dynamics and molecular reorientation processes in ferroelectric liquid crystals, Rev. Sci. Inst. 59 (1988) 2023-2030.

[85] S.A. Arrhenius, On the reaction rate of the inversion of non-refined sugar upon souring, Z. Phys. Chem. 4 (1889) 99-116.